Journal of Electronics and Electrical Engineering
https://ojs.wiserpub.com/index.php/JEEE/

Article

Research on Solenoid Valve Plunger Detection System for Automotive Powertrain Applications

Borislav Dimitrov and Mohammadali Abbasian

University of Warwick, WMG, Coventry, CV4 7AL, the UK
E-mail: Borislav.Dimitrov@warwick.ac.uk

Received: 15 May 2025**; Revised:** 23 July 2025**; Accepted:** 30 July 2025

Abstract: The research presents a design for a power supply system specialised in supplying a solenoid electromechanical system, which is a crucial component in automotive applications, including electric vehicles. The implementation of plunger position monitoring, a key feature according to functional safety standards, is organised with a microprocessor system to satisfy the Functional Safety (FS) requirements. The proposed system's topology aims to achieve Quality Management (QM) for the monitored electromechanical system at ASIL B or ASIL D (Automotive Safety Integrity Level), potentially advancing the automotive industry. The developed monitoring system incorporates two independent plunger detection mechanisms based on current measurement, calculation, and plunger estimation. The suggested power supply is based on a modified Forward converter with an adjusted structure and design methodology tailored to the solenoid characteristics. The obtained results are presented analytically and supported by experimental verification, paving the way for potential advancements in the automotive industry.

Keywords: Solenoid, Electric Vehicles, Functional Safety, ISO26262, Actuator, Forward converter

Nomenclature

Term	Description
FS	Functional Safety
QM	Quality Management
ASIL	Automotive Safety Integrity Level
EV	Electric Vehicles
V2G	Vehicle-To-Grid
ASIC	Application Specific Integrated Circuit
MU	Microcontroller unit
PM	Primary Microcontroller
SM	Secondary Microcontroller
VCU	Vehicle Control Unit
ESR	Functional Safety Requirements
FTTI	Fault-Tolerant Time Interval (FTTI)
I_{PEAK}	Peak current of the solenoid(A)
I_{VALLEY}	Valley current of the solenoid (A)
I_{MAX}	Maximum current of the solenoid (A)
L	Inductance of the solenoid (H)
w	Number of coil turns
μ_o	Permeability
d	Plunger diameter (m)

DOI: https://doi.org/10.37256/10.37256/jeee.4220257243

δ	Plunger air gap (m)
V_{out}	Forward converter output voltage (V)
V_{in}	Forward converter input (V)
N_{pri}	Primary transformer turns
N_{sec}	Secondary transformer turns
η	Forward converter efficiency
F_{sw}	Forward converter switching frequency (Hz)
t_{on}	On-time of the MOSFET (s)
$I_{out(rip)}$	Output current ripple
$V_{out(rip)}$	Output voltage ripple

1. Introduction

Solenoid electromagnets [1-6] are essential components in the electric drivetrain, including Electric Vehicles (EVs) today. Their design [1, 2] and optimisation [3, 4] are vital for advancing the electric drivetrain, making our research on the solenoid power supply system highly important. Their analysis [5, 6] involves identifying key electromagnetic system characteristics and ensuring solenoid performance in the required environment.

The solenoids' power supply system establishes interface compatibility between the power source and the coil's parameters. In an EV application, a DC-DC converter could be integrated. To determine its specifications, the following requirements could be systematised: 1) high-to-low voltage conversion from the EV battery (up to 800V) to the actuator operating at 12V or 24V; 2) a transformer-based converter providing galvanic isolation between primary and secondary sides; 3) high power density, reliability, and efficiency; 4) electromagnetic compatibility. Based on recent research, the Forward converter offers proven advantages for EV applications as an auxiliary power supply, potentially for actuators. Although it is a well-known topology, the Forward converter still has significant research potential. In [7], an alternative bi-directional Forward converter is proposed as part of the Vehicle-To-Grid (V2G) system. The converter achieves 94.21% efficiency in forward mode and 93.78% in regenerative mode. Other recent sources present improved design procedures based on modelling [8, 9] with advanced mathematical tools, leading to better efficiency and lower noise [10]. An efficiency enhancement for the forward converter could be achieved with the resonant topology suggested in [11], which shows that high-to-low voltage (400V/20V) conversion can reach up to 95% efficiency at 65W. GaN HEMT transistors could be used as an alternative solution, including as part of the active clamp, as shown in [12].

As part of the EV, solenoid systems are subject to functional safety analysis according to the standard ISO26262 [13]. Depending on their position in the electric drivetrain, the required safety level can range from QM (Quality Management) to ASIL (Automotive Safety Integrity Level) A, B, C, or D, with the safety level increasing from ASIL A to D. The development and verification of the ASIL level [14, 15, 16], based on expert scrutiny supported by software tools and model-based engineering, is a crucial aspect of the entire drivetrain design. Since power converters are central to the electric drivetrain [17], their emergency operation and integrated redundancy must also be considered for the solenoid's power supply to meet the required ASIL level. In this context, fault detection [18] is a mandatory component of solenoid operation, ensured through plunger position detection. This mechanism should be based on microcontrollers rated at ASIL B or ASIL D, which measure and estimate the plunger position using two or more independent detection methods.

This research aims to develop and complete the solenoid electromagnetic system for EV applications, including plunger detection analysis, power supply design, and experimental verification. Therefore, the proposed system should include a topology supporting ASIL B and D requirements for plunger detection. The solenoid power supply meets the QM level and is achieved through adjustments in topology and design methodology based on the specific characteristics of the solenoid.

The rest of the paper is organised as follows: Section 2 describes the system structure and provides an overview of the functional safety requirements; Section 3 presents the mechanism for plunger detection; Section 4 outlines the design process of the solenoid's power supply DC-DC converter; experimental verification is discussed in Section 5; and the conclusions are given in Section 6.

2. System analysis

The topology of the suggested system (Fig. 1) consists of the following units:

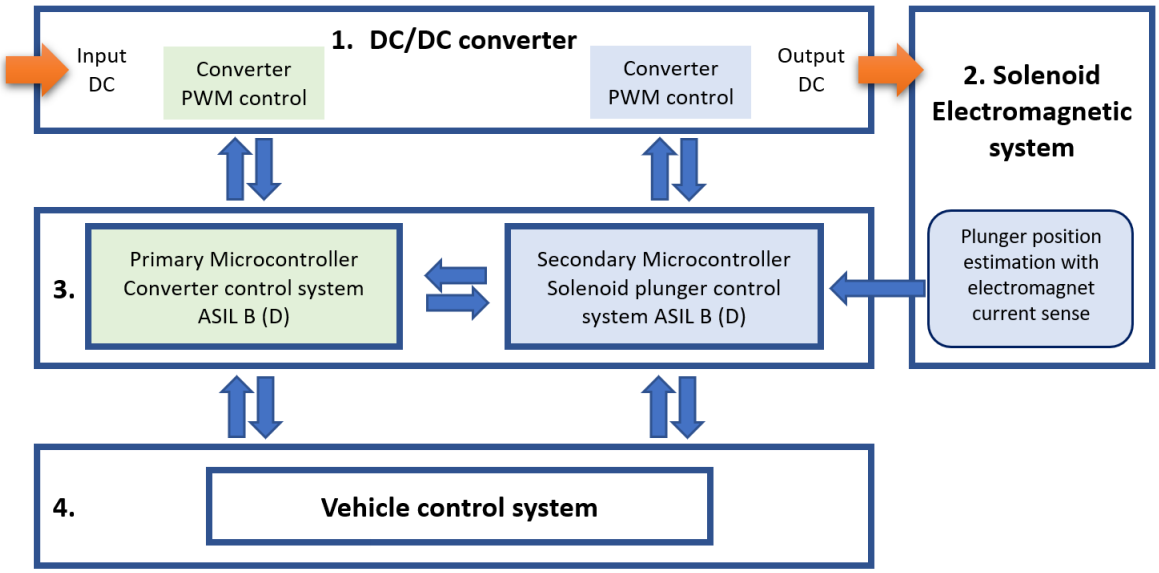

Figure 1. The general concept of the suggested system for solenoid plunger position estimation.

1. DC/DC converter. A Forward topology is chosen, controlled by an Application Specific Integrated Circuit (ASIC) capable of communicating its status through two channels—either to two independent ASIL D microcontrollers or to an ASIL B microcontroller with two cores. The Forward converter must meet QM requirements, transforming high voltage (HV), potentially from the EV main battery, to low voltage (LV), suitable for solenoid coil DC voltage. To achieve this, the power section of the Forward converter topology is modified by removing the output filter, as shown in Section 4.
2. The solenoid electromagnetic system. It is a standard solenoid electromagnet [1-6] used to energise the actuators for EV applications. The coil is equipped with current sensors to provide the necessary feedback signal.
3. Microcontroller unit (MU). It can be divided into two independent ASIL D microcontrollers or a single two-core SDIL B microcontroller, which independently estimates the plunger position according to the methodology presented in the next section. In both feasible topologies, the plunger estimation is performed by the Primary Microcontroller (PM) and the Secondary Microcontroller (SM) to ensure the required ASIL.
4. Vehicle Control Unit (VCU). The solenoid status is communicated with the vehicle control system (out of scope in this research).

The main Functional Safety Requirements (FSR) to satisfy ASIL D for the plunger detection and the QM for the DC/DC converter are arranged as follows:

1. The MU shall analyse the request from the VCU for the solenoid ON or OFF status.
2. The MU shall receive the current status from the solenoid feedback and analyse the plunger position.
3. The PM and SM shall detect the same status, supplying the signal to the DC/DC converter with two independent channels.
4. The MU shall return fault status to VCU if a mismatch is detected.
5. The DC/DC converter shall compare the signals from the PM and SM.
6. If a mismatch is detected, the DC/DC converter shall return a fault status to the VCU.
7. The DC/DC converter shall supply the solenoid with the required DC voltage and current.
8. The DC/DC converter shall ensure galvanic isolation on the primary-to-secondary side.
9. The MU shall estimate the plunger position by detecting three current points: peak I_{PEAK}, valley I_{VALLEY} and maximum I_{MAX} during the Switch-ON solenoid transient process.
10. The UM shall estimate the transient Switch-OFF process with mechanical switches detecting the plunger's initial position.

The Fault-Tolerant Time Interval (FTTI) is 30-100 ms, comparable to solenoid Switch-ON and Switch-OFF times. With this tolerance, the alarm signal can be communicated with the VCU after completing the transient process.

3. Solenoid plunger detection

Fig. 2 illustrates the solenoid electromagnetic system. Its main components are the excitation coil supplied from the power supply system (Section 4), a steel frame acting as an electromagnetic flux conductor, a plunger to apply force to the actuator, and a spring to return the plunger to its initial position.

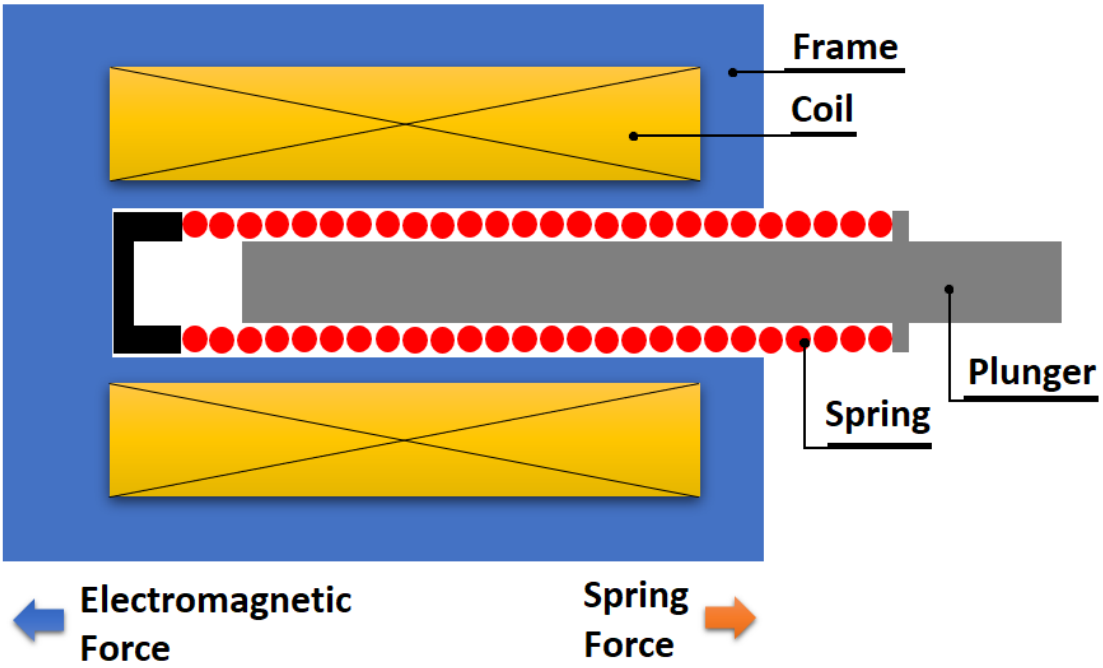

Figure 2. Solenoid electromagnetic system.

When the electromagnet is energised, the coil's current rises during the transient period, as shown in Fig. 3. The diagram can be divided into three sections, product of the plunger movement profile: 1) $0A - I_{PEAK}$ The current rises, increasing the electromagnetic force, causing the plunger to start moving at I_{PEAK}; 2) $I_{PEAK} - I_{VALLEY}$ The plunger is moving, inducing back EMF, which causes a current reduction to the point of I_{VALLEY}. 3) $I_{VALLEY} - I_{MAX}$ The current rises to its maximum point I_{MAX}, limited by the electromagnetic coil resistance. The described critical points I_{PEAK}, I_{VALLEY} and I_{MAX} in the current transient process are essential for the plunger position estimation.

Given the above considerations, the plunger position can be determined by the current deviation caused by the change in inductance. For this purpose, the fundamental equation of the solenoid system needs to be defined as:

$$V = Ri + \frac{d\Psi}{dt} = Ri + L\frac{di}{dt} + i\frac{dL}{dt} \quad (1)$$

where: V is the voltage applied to the coil; R is the coil resistance; i is the current; Ψ is the flux linkage; L is the inductance.

As the equation shows, the plunger's position will determine the coil's inductance, hence the linkage flux. The electromagnetic force F is given by:

$$F = \frac{1}{2}(iw)^2\mu_o\frac{\pi d^2}{4\delta^2} \quad (2)$$

where: i is the current; w is the number of coil turns; μ_o is the permeability; d is the plunger diameter; δ is the air gap.

The current at the start conditions of the transient process (Fig. 3, section $0A - I_{PEAK}$) will be described with the equation:

$$i = I_o(1 - e^{-t/T}) \quad (3)$$

where: $I_o = V/R$

Respectively, the time constant at the starting process will be described as:

$$t = Tln\frac{1}{1-\frac{i}{I_o}} \quad (4)$$

The presented equations (1-4) describe the current diagram in Fig. 3, highlighting three key points. An approach for plunger movement involves their predefinition, consistent current measurements throughout the entire transient process, and comparison with both microcontrollers (Fig. 1). This also requires measuring the coil's temperature, which could compromise functional safety by adding another sensor with necessary redundancy. As shown in Fig. 4, the transient process is temperature-sensitive, since the coil's resistance variation causes current variation.

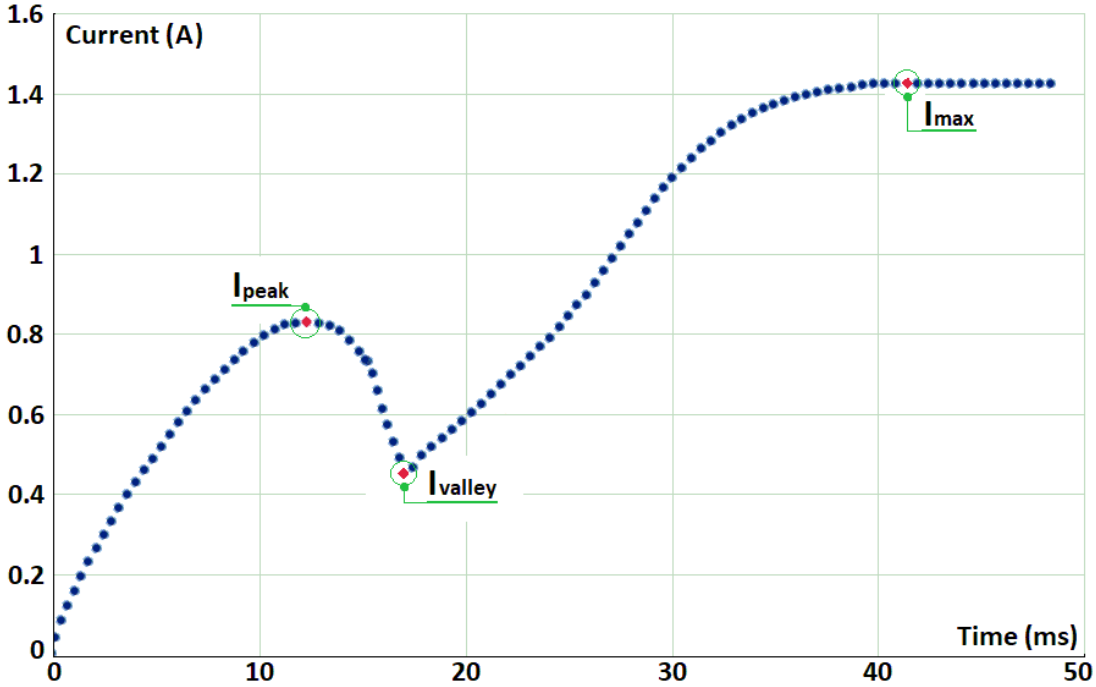

Figure 3. Current through the electromagnet system coil. Switch-on transient process.

The suggested system estimates the plunger movement by measuring the current points (Fig. 4) and calculating the current differences $I_{PEAK} - I_{VALLEY}$ and $I_{MAX} - I_{VALLEY}$. Such an approach eliminates the need for precise current determination and temperature measurement.

During the transient process, it can be expected that the current differences between I_{PEAK} and I_{VALLEY} will remain constant despite the temperature variations. However, the preliminary measurements show that some current deviation is possible due to multiple factors such as resistance nonlinearity, friction, temperature impact on the actuator, etc. Table 1 shows measured currents at different ambient temperatures at initial conditions, showing the variation in the currents I_{PEAK}, I_{VALLEY} and I_{MAX}. As can be seen, the current difference between $I_{PEAK} - I_{VALLEY}$ and $I_{MAX} - I_{VALLEY}$ varies within 8-12% between the two extreme temperatures. Such variations must be determined for the investigated electromagnetic system, including the actuator, and implemented in the microcontroller's calculation algorithm.

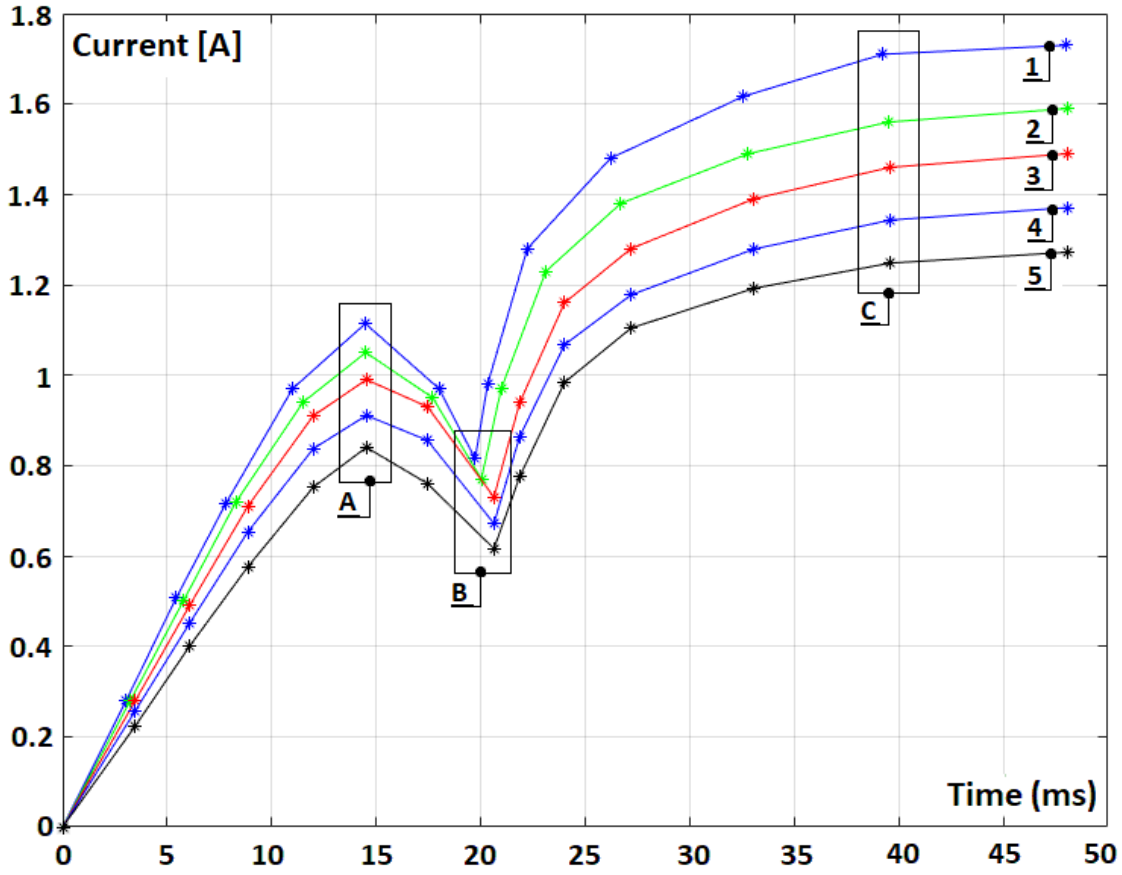

Figure 4. Coil's current variation with the temperature. 1: -10^oC; 2: 0^oC; 3: 20^oC; 4: 40^oC; 5: 50^oC. Section A: variation of the I_{PEAK}; Section B: variation of the I_{VALLEY}; Section C: variation of the I_{MAX}

Table 1. Measured current points and differences for the transient electromagnet switch-on process

Temperature °C	-10	0	20	40	50
I_{PK}	1.1	1.05	0.99	0.91	0.86
I_{VALL}	0.83	0.78	0.73	0.66	0.61
I_{MAX}	1.6	1.5	1.5	1.3	1.3
$I_{PK} - I_{VALL}$	0.27	0.27	0.26	0.25	0.25
$I_{MAX} - I_{VALL}$	0.77	0.77	0.77	0.64	0.69

Another possible level of variation is in the time of measurement. For the presented data (Fig. 4, Table 1), the peak current I_{PEAK} varies in a narrow range of $14.2 - 14.8\,ms$, respectively I_{VALLEY} in a range of $19.5 - 21.1ms$ and I_{MAX} are measured in a range of $38 - 39ms$.

4. The solenoid power supply system design

The power supply is an indispensable part of the suggested system, serving as an object of monitoring and control according to the FSR. In the developed system, a forward topology was chosen. The proposed modification removes the secondary side output filter (L1, C2), which is mandatory in the general topology, and supplies the solenoid system Ls with only two rectifiers. This reduction in passive elements enhances power density, efficiency, and overall system reliability.

The design methodology utilised relies on a step-by-step approach, applied in accordance with the suggested converter modification (Fig. 5).

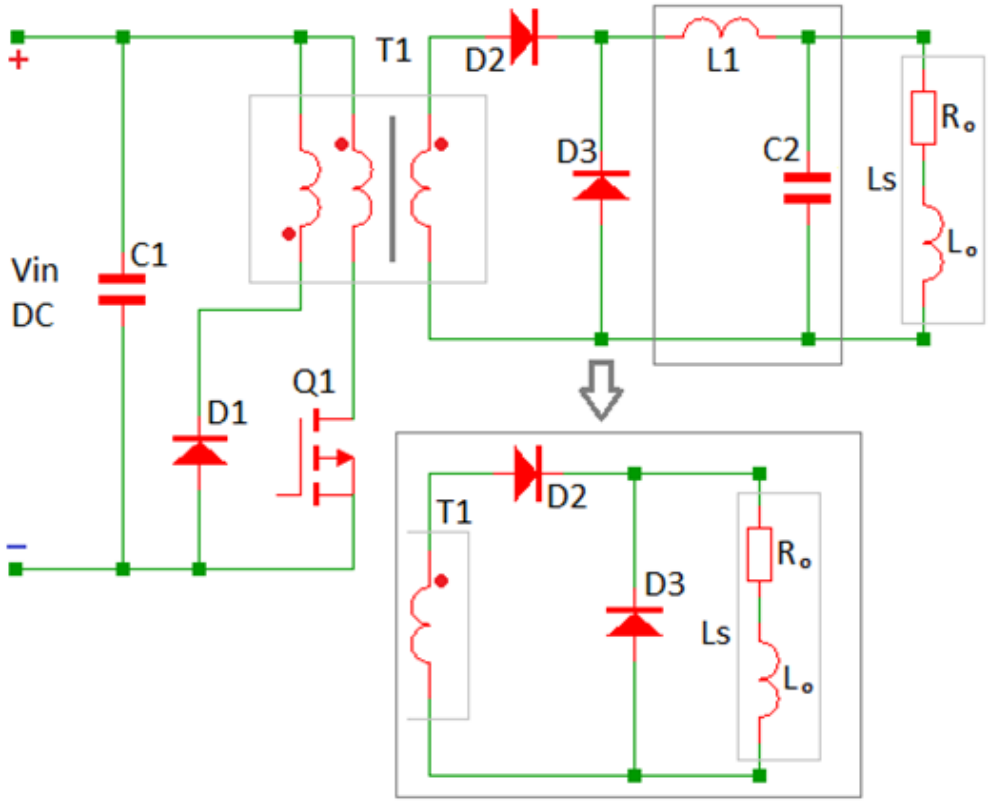

Figure 5. Forward converter secondary side modification for the supply of the solenoid system

The criteria for the winding ratio N_{sec}/N_{pri} determination is the output voltage to be executed at the maximum duty cycle DC. Including the winding ratio in the buck gain $V_{out} = V_{in} \times DC$, the forward gain can be written as:

$$\frac{V_{out}}{V_{in}} = \frac{N_{sec}}{N_{pri}}.DC \quad (5)$$

were V_{out} and V_{in} are respectively the output and the input voltage; N_{sec} and N_{pri} are the secondary and primary numbers of turns.

The On-time t_{on} can be determined from these ratios and the switching frequency F_{SW}:

$$t_{on} = \frac{V_{out}}{V_{in}}.\frac{N_{pri}}{N_{sec}}.\frac{1}{F_{sw}} \quad (6)$$

The primary number of turns is calculated based on the transformer T1 core parameters as follows:

$$N_{pri} \geq \frac{V_{in}.DC}{B_{max}.A_e.F_{sw}} \quad (7)$$

were B_{max} is the maximum flux density, and A_e is the required area.

Due to the output L1-C2 filter removal, the solenoid L_S acts as the converter loads, applying its inductance L_o and resistance R_o. The expected output current ripples Δi_{rip} can be derived from the equation:

$$L_s = \left(1 - \frac{V_{out}}{V_{in}}.\frac{N_{pri}}{N_{sec}}\right).\frac{V_{out}}{\Delta i_{rip}.F_{sw}} \quad (8)$$

considering that L_s is preliminarily determined as a solenoid parameter:

$$\Delta i_{rip} = \left(1 - \frac{V_{out}}{V_{in}}.\frac{N_{pri}}{N_{sec}}\right).\frac{V_{out}}{L_s \times F_{sw}} \quad (9)$$

The mean value of the primary current should be calculated based on the expected converter's overall efficiency $\eta = P_{out}/P_{in}$. A realistic expectation, taking into account the L1-C2 reduction, could be $0.85 \leq \eta \leq 0.9$. Therefore, the primary side mean current $I_{prim,mean}$ will be:

$$I_{prim,mean} = \frac{P_{out}}{\eta.V_{in} \times DC} = \frac{P_{in}}{V_{in}.DC} \quad (10)$$

where P_{out} and P_{in} are respectively the output and input power.

The primary peak current in the demagnetising winding (N_{mag}) is:

$$\Delta i_{prim,peak} = \frac{\Delta i_{rip} \cdot I_{prim,mean}}{2.I_{Ls,max}} \quad (11)$$

where $I_{Ls,max}$ is the maximum solenoid current.

The peak current value through the transistor Q1 is reached at the end of the period t_{on}, calculated from the equation:

$$\Delta i_{Q_1} = \frac{V_i . t_{on}}{L_M} \quad (12)$$

where L_M is the primary side transformer inductance.

The sum of the last three equations (6, 7, 8) provides the total maximum peak primary current:

$$I_{S,peak} = I_{prim,mean} + \Delta i_{prim,peak} + \Delta i_{Q1} \quad (13)$$

Q1 RMS current is expressed with the equation:

$$I_{s,rms} = I_{prim,mean} . \sqrt{DC} . \sqrt{1 + \frac{\left(\frac{\Delta i_{prim,peak} + \left(\frac{\Delta i_{Q_1}}{2} \right)}{I_{prim,mean}} \right)^2}{3}} \quad (14)$$

The calculated $I_{s,rms}$ value is used to determine the conducting $P_{S,cond}$ and switching P_{SW} power loss as follows:

$$P_{S,cond} = I_{S,rms}^2 . R_{on} \quad (15)$$

$$E_{ON} = \frac{I_{s,rms} . V_{in}}{2} . \left(t_{d(on)} + t_{r(on)} \right) \quad (16)$$

$$E_{OFF} = \frac{I_{s,rms} . V_{in}}{2} . \left(t_{d(off)} + t_{f(off)} \right) \quad (17)$$

$$P_{SW} = (E_{ON} + E_{OFF}) . F_{SW} \quad (18)$$

where E_{ON} is the on-energy, calculated from the datasheet timing $t_{d(on)}$ time ON-delay and $t_{r(on)}$ rise time; E_{OFF} is the off-energy, calculated from the datasheet timing $t_{d(off)}$ time OFF-delay and $t_{f(off)}$ fall time.

Ultimately, the total transistor loss will be represented by the sum of the conducting and switching losses, expressed by the equation:

$$P_{S,total} = P_{S,cond} + P_{SW} \quad (19)$$

The diode D1 demagnetisation current is calculated from:

$$I_{D1,demag} = \frac{V_{in} . t_{on}}{L_M} \quad (20)$$

The diode D1 RMS current is calculated from:

$$I_{D1,RMS} = I_{D1,demag} . \sqrt{\frac{DC}{3}}, \quad (21)$$

with the diode conducting loss:

$$P_{D1} = I_{D1,max} . V_F \quad (22)$$

Considering an equal number of turns in N_{pri} and N_{mag}, i.e. the turn ratio is $\frac{N_{pri}}{N_{mag}} = 1$ the reverse D1 voltage can be calculated from:

$$V_{D1} > 1.1 . V_{in} \quad (23)$$

The maximum voltage can be estimated with a 20% safety design margin, used for diode selection:

$$V_{D1,max} \geq 1.2 . V_{D1} \quad (24)$$

The maximum reverse voltage estimation for both diodes D2 and D3 can be calculated using the equation:

$$V_{D2,D3} > 1.1 . \left(V_{i,max} . \frac{N_{sec}}{N_{pri}} - V_F \right) \quad (25)$$

with a safety design margin, the criteria for D2 and D3 voltage selection is:

$$V_{D2,D3,max} \geq V_{D2,D3} . 1.2 \quad (26)$$

Both current RMSs will be given with the equation:

$$I_{D2,D3} = \frac{I_{Ls}}{\sqrt{2}} \quad (27)$$

The conductive and switching (reverse-recovering) power losses of both diodes will be determined:

$$P_{D2,D3,cond} = I_{L_S} . V_F \quad (28)$$

$$P_{D2,D3,sw} = \frac{V_{D2,D3,max} . Q_{rr} . F_{SW}}{3} \quad (29)$$

Where the Q_{rr} is the diodes' reverse recovery charge.

$$P_{D2,D3,total} = P_{D2,D3,cond} + P_{D2,D3,sw} \quad (30)$$

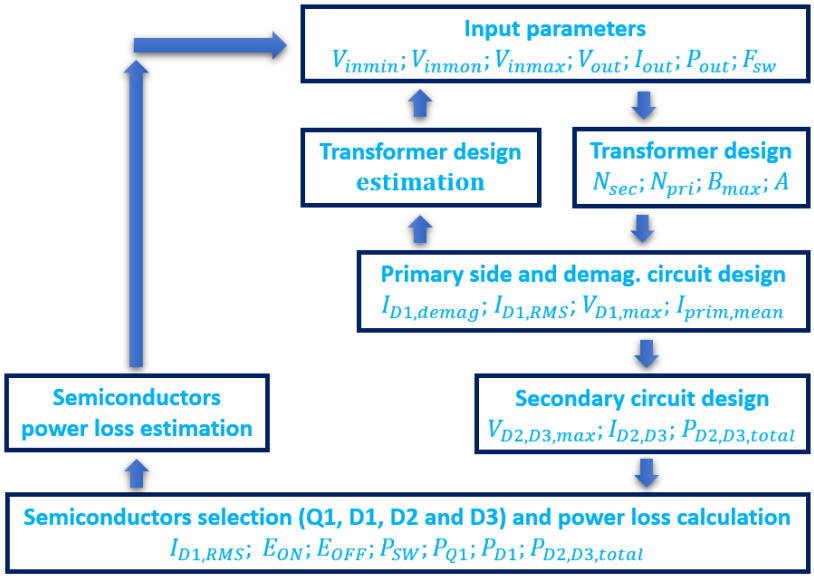

Figure 6. A flow chart illustrating the design process.

Forward converter input design parameters:

- Input voltage range $200V \leq V_{in} \leq 400V$
- Output voltage $V_{out} = 12V$
- Output current $I_{out} = 2A$
- Output power $P_{out} = 24W$
- Switching frequency $F_{sw} = 100kHz$
- Maximum duty cycle $DC = 50\%$

The flowchart in Fig. 6 offers a visual representation of the design process described. Based on the input parameters accepted above, the final results are provided in Table 2.

Table 2. Forward converter design results

Equations	Results
5, 6, 7, 8	$N_{pri} = 69; N_{sec} = 4; t_{on} = 5\mu s; B_{max} = 0.3; A_e = 97.1 \times 10^{-6}$
9, 10, 11	$\Delta i_{rip} = 0.58A; I_{prim,mean} = 0.14A; \Delta i_{prim,peak} = 0.02A$
12, 13, 14	$\Delta i_{Q_1} = 0.74A; I_{S,peak} = 0.9A; I_{s,rms} = 0.19A$
15, 16, 17	$P_{S,cond} = 109.8\,mW; E_{ON} = 0.68\,\mu J; E_{Off} = 2.26\,\mu J$
18, 19	$P_{SW} = 293.6\,mW; P_{total} = 0.4W$
20, 21, 22, 23, 24	$I_{D1,demag} = 0.74A; I_{D1,RMS} = 0.3A; P_{D1} = 0.52W; V_{D1} > 440V; V_{D1,max} \geq 528V$
25, 26, 27	$V_{D2,D3} > 24.96V; V_{D2,D3,max} \geq 29.95V; I_{D2,D3} = 1.4A$
28, 29, 30	$P_{D2,D3,cond} = 1W; P_{D2,D3,sw} = 8.3mW; P_{D2,D3,total} = 1W$

The selected semiconductors used for the experimental verification prototypes are as follows: Q1 – IPP60R099C6XKSA1 (TO-220 package) or IPD80R1K4P7 (DPAC package); D1 – MURS160T3G (SMD); D2, D3 – MBRS340T3G (SMD).

5. Experimental verification

The experimental verification was conducted in the following order: 1) the suggested system was designed, including the DC/DC converter and MU; 2) a standard low-voltage vehicle solenoid actuator was used, additionally equipped with current sensors; 3) the VCU was physically emulated to detect the conducted emergency signals and to measure the obtained time constants; 4) the system was tested, and the oscillograms were recorded to visualise its operation; 5) the thermal operation of the designed forward converter was tested and recorded with an infrared camera. The experimental results are visualised in Fig. 7 – Fig. 13 as follows:

Fig. 7 shows the transient process of the experimentally tested solenoid, where diagram 1 represents the voltage applied to the coil and diagram 2 depicts the current through the coil. The process is completed for the time T2 = 35ms, giving a peak current $I_{peak} = 2A$ and valley current $I_{valley} = 1.6A$ at the time $T1 = 17ms$. The maximum current at the steady-state conditions reaches $I_{max} = 2.45A$. The experiment shows the transient process's leading conditions; therefore, the measured data have been used to adjust the MU's time parameters.

Fig. 8 shows the transient process with the lock-up plunger. The MU detected this condition and communicated the emergency signal (diagram 3) to the VCU. The time for this operation is equal to the transient process, e.g., T1=35ms. With this, the statement above, according to the FTTI parameter, is satisfied.

Fig. 9 shows the operation of the designed and prototype forward DC/DC converter with the suggested modification following Fig. 5. Drain-to-source Q1 voltage is displayed in diagram 1. The oscillations are acceptable; however, they could be reduced with an additional snubber circuit. The operation of the primary-side diode D1 appears in diagram 2. Transformer core demagnetisation occurs during the transistor's off-time. The PWM control signal to transistor Q1 is shown in diagram 3, with a maximum duty cycle of 48%, and the MOSFET current is illustrated in diagram 4. Fig. 10 depicts the current through the demagnetisation diode D1 as part of the primary converter side experimental study. Diagrams 2, 3, and 4 correspond to those in Fig. 9.

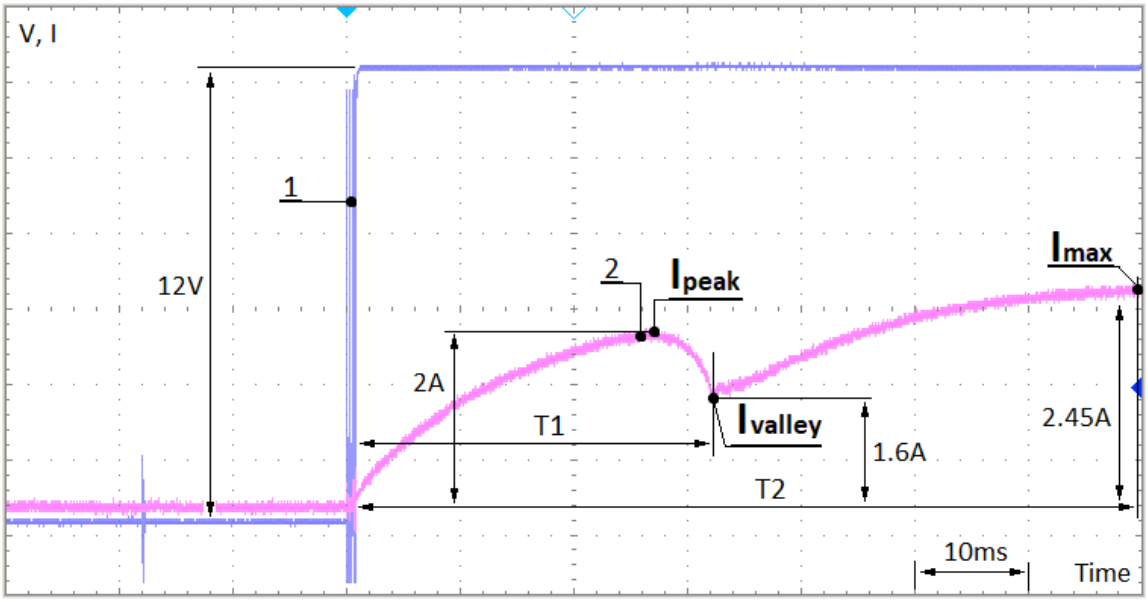

Figure 7. Switching on the transient process of the solenoid. 1- Voltage; 2-Current; T1=17ms; T2=35ms; $I_{peak} = 2A$; $I_{valley} = 1.6A$; $I_{max} = 2.45A$

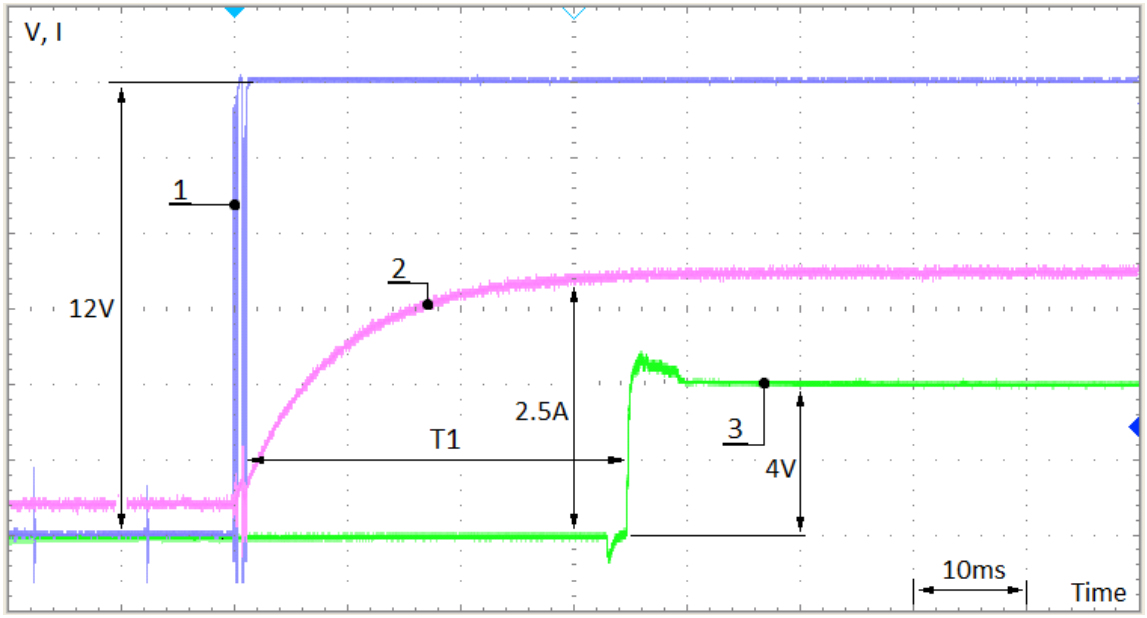

Figure 8. Switching on the transient process of the solenoid with a lock-up plunger. 1- Voltage; 2-Current; T1=35ms; 3-emergency signal conducted to the VCU.

The operation of the converter's secondary side with the inductor L1 and the electrolytic capacitor C2 removed is shown in Fig. 11. The voltage over the solenoid and the current through it are shown, respectively, with diagrams 1 and 4. The current ripples in these conditions do not exceed 20-25% due to the freewheeling operation supported by the diode D3. Diagram 2 shows the transformer secondary side voltage, and diagram 3 shows the primary side PWM for synchronisation.

The achieved result guarantees the solenoid's stable operation without plunger vibrations. Nonetheless, further improvements are possible by connecting a ceramic capacitor in parallel with the actuator coil (C2, Fig. 5). For this experiment, an SMD ceramic capacitor of 1µF and 24V is used, calculated by the following equation:

$$C_{out} = \frac{I_{out(rip)}}{8.F_{sw}.V_{out(rip)}} \quad (31)$$

where $I_{out(rip)}$ is the output current ripple (10 mA); $V_{out(rip)}$ is the output voltage ripple (12 mV).

As shown in the last oscillogram, the proposed modification significantly reduces the output ripples while still meeting the requirement for increased power density by removing the input inductor and electrolytic capacitor.

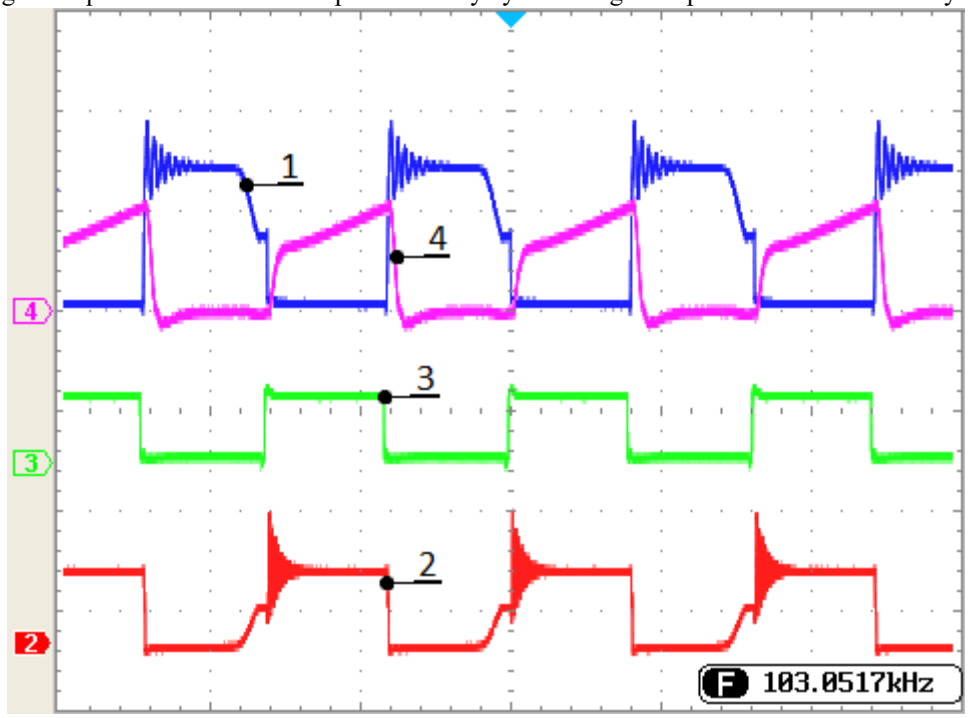

Figure 9. DC-DC converter primary side experimental verification. 1 – Q1 Drain-Source voltage; 2 – D1 voltage; 3 – PWM; 4 – Q1 Drain current.

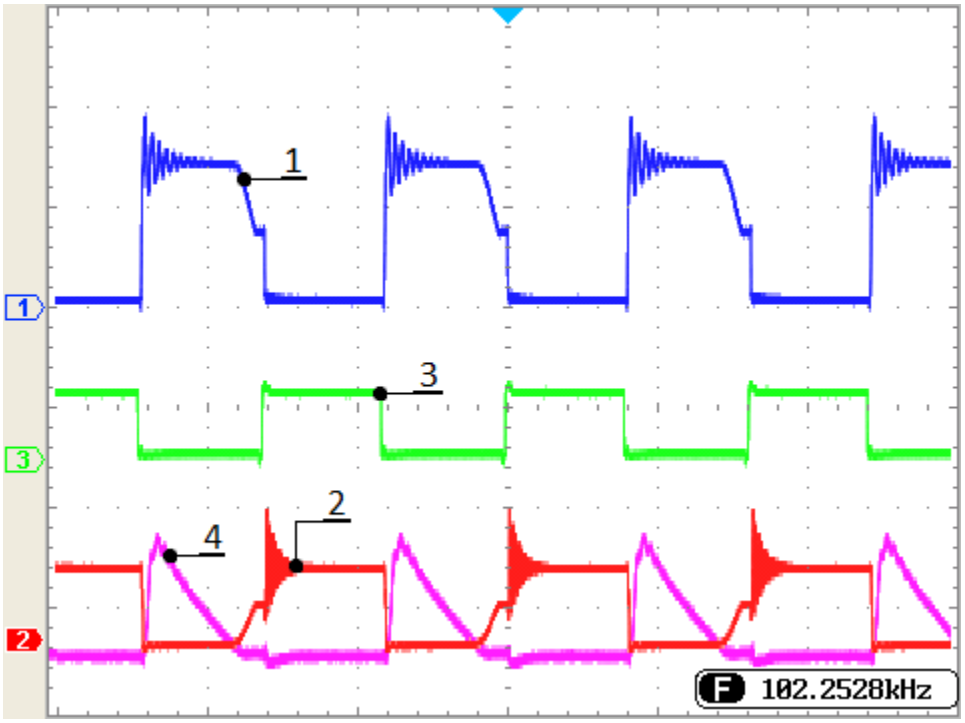

Figure 10. DC-DC converter primary side experimental verification. 1 – Q1 Drain-Source voltage; 2 – D1 voltage drop; 3 – PWM; 4 – D1 current.

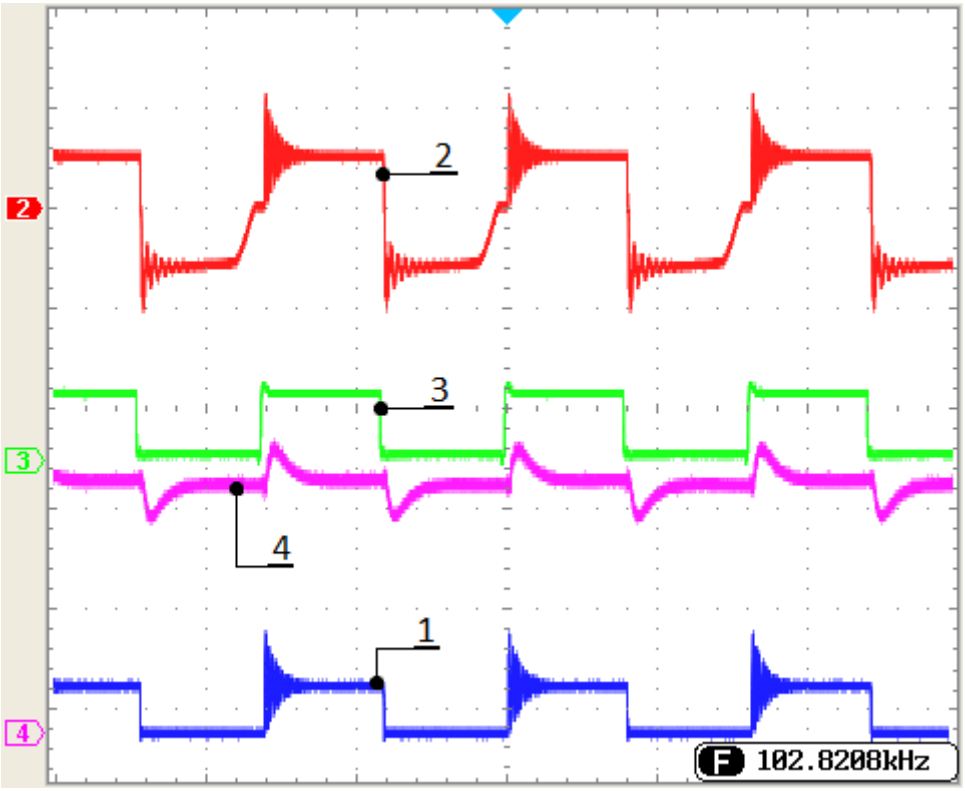

Figure 11. DC-DC converter secondary side experimental verification. 1 – Solenoid voltage; 2 – T1 secondary side voltage; 3 – PWM; 4 – Solenoid current.

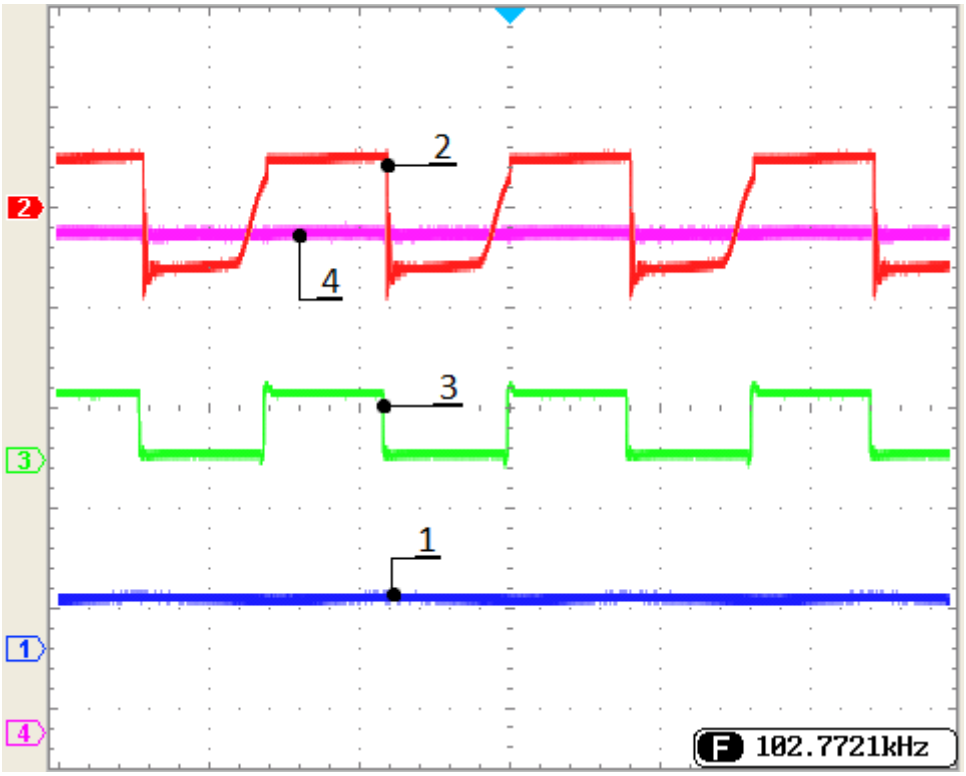

Figure 12. DC-DC converter secondary side experimental verification with added capacitor C2. 1 – Solenoid voltage; 2 – T1 secondary side voltage; 3 – PWM; 4 – Solenoid current.

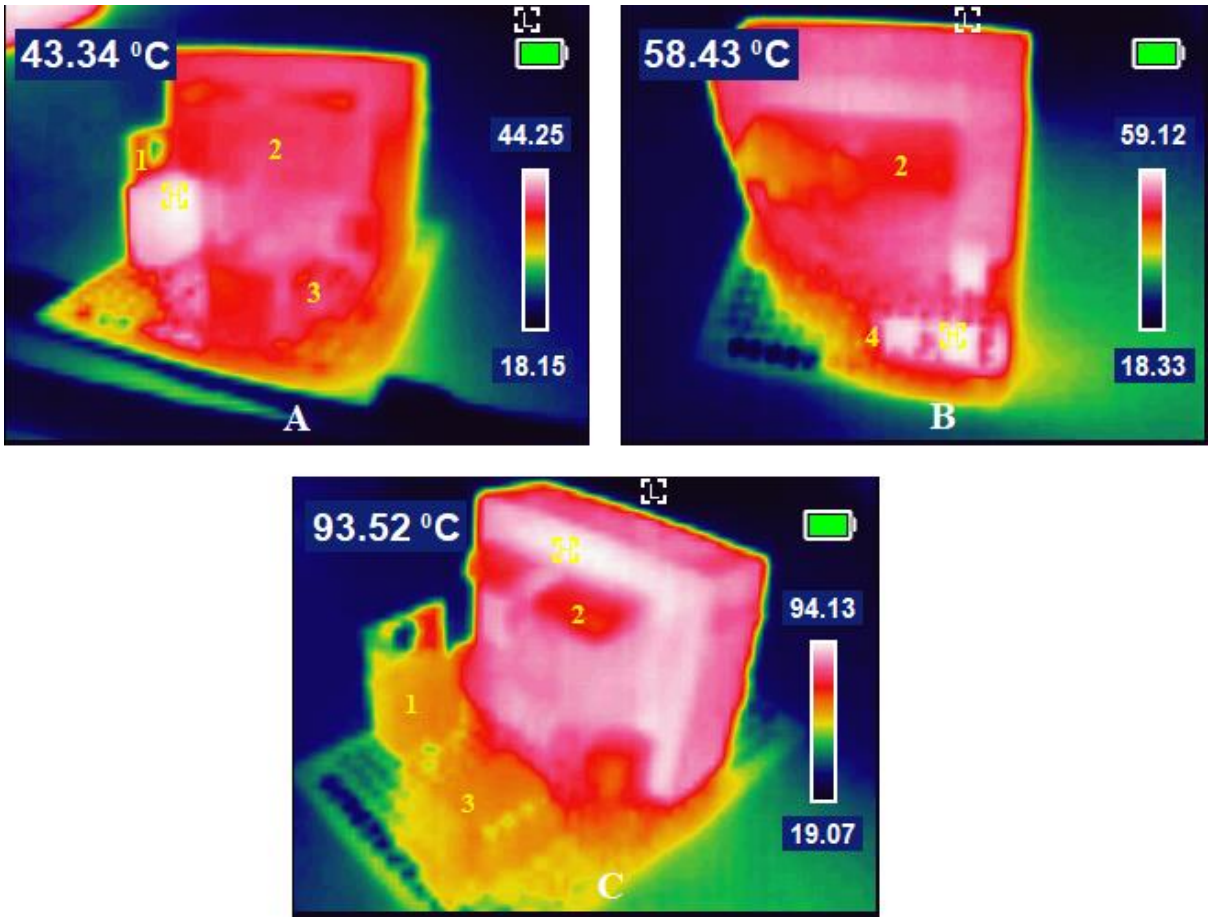

Figure 13. Thermal operation of the designed forward converter. 1 MOSFET; 2 – Transformer; 3 – ASIC (out of scope in this design); 4 – secondary side rectifier.

Finally, Fig. 13 illustrates infrared thermal images of the prototyped converter. The measured temperatures in the main components are as follows: MOSFET (Q1) 43.34^oC, secondary side rectifier (D2) 58.43^oC, transformer core (T1) 93.52^oC. The steady-state temperatures recorded for the transistor (A), rectifier (B), and transformer (C) are acceptable.

6. Conclusions

This research presented a study on a solenoid plunger detection system applicable to automotive drivetrains, achieving an ASIL B or ASIL D classification according to ISO26262. The proposed topology (Fig. 1) demonstrated stable operation in plunger detection, supported by two independent microcontrollers to meet the redundancy requirements of ASIL D. The emergency signal was sent to the VCU due to the lock-up of the immovable plunger. These results confirm the achieved functional safety level in [7-12], satisfying the FS requirements with a modified converter topology.

The designed and experimentally tested forward converter matched the solenoid interface with the recommended modification. Removing the output filter (L1, C2) also improved the converter's power density, which is crucial for automotive applications. The forward converter's overall operation aligns with the designed procedures [7-12], while the research extended them further in the specific application described. Therefore, the presented design methodology can be regarded as a valuable approach specifically related to the system investigated.

Conflict of interest

There is no conflict of interest for this study.

References

[1] M. Mauch and B. Gundelsweiler, “Design of a hybrid electromagnetic switching/holding solenoid with adjustable core,” IKMT 2022; 13. GMM/ETG-Symposium, Linz, Austria, 2022, pp. 1-6.

[2] T. Braun, J. Reuter and J. Rudolph, “Observer Design for Self-Sensing of Solenoid Actuators With Application to Soft Landing,” in IEEE Transactions on Control Systems Technology, vol. 27, pp. 1720-1727, 2019

[3] E. Plavec and M. Vidović, “Genetic algorithm based plunger shape optimisation of DC solenoid electromagnetic actuator,” 2016 24th Telecommunications Forum, Belgrade, 2016, pp. 1-4.

[4] S. Wu, et al, “Multiobjective Optimisation of a Hollow Plunger Type Solenoid for High-Speed On/Off Valve,” in IEEE Transactions on Industrial Electronics, vol. 65, no. 4, pp. 3115-3124, 2018.

[5] Lulu Huang, Hong Ji and Yi Zhu, “Analysis of effective working characteristic of the proportional solenoid,” 2017 International Conference on Green Energy and Applications, Singapore, 2017, pp. 35-38.

[6] W. Enomoto, S. Yokota, K. Matsumoto, D. Chugo, S. Muramatsu and H. Hashimoto, “Feasibility Study on Ungrounded Pulling Force Display Using Electromagnetic Force of Solenoid,” 2024 IEEE/SICE International Symposium on System Integration, Ha Long, Vietnam, 2024, pp. 840-844.

[7] C. Chaudhari, M. Bagewadi and S. Dambhare, “A Novel Dual Active Forward Converter Based Bidirectional Multiport Converter for EV Applications,” 2022 4th International Conference on Smart Power & Internet Energy Systems, Beijing, China, 2022, pp. 824-829.

[8] P. Mundotiya, A. Koli, N. Goyal, G. Kansotia, N. Meena and H. Tiwari, “A Novel Mathematical Modelling Technique for Control of DC-DC Forward Converter,” 2024 3rd International Conference on Power Electronics and IoT Applications in Renewable Energy and its Control, Mathura, 2024, pp. 141-146.

[9] D. Lee, et al., “Derivation and Analysis of New Small-Signal Model for Active Clamp Forward Converter,” 2024 IEEE Applied Power Electronics Conference and Exposition, Long Beach, CA, USA, 2024, pp. 606-611.

[10] S. K. Tummala and L. Duraiswamy, “Switched Mode Power Supply: A High Efficient Low Noise Forward Converter Design Topology,” IEEE 2nd International Conference on Sustainable Energy and Future Electric Transportation, Hyderabad, 2022, pp. 1-5.

[11] H. Peng et al., “A novel and simple hybrid DC-DC converter of resonant forward and PWM flyback,” 2018 IEEE Applied Power Electronics Conference and Exposition, San Antonio, USA, 2018, pp. 1520-1527.

[12] Ö. Bulut and M. T. Aydemir, “Design and loss analysis of a 200-W GaN based active clamp forward converter,” 2018 5th International Conference on Electrical and Electronic Engineering, Istanbul, 2018, pp. 97-100.
[13] https://www.iso.org/standard/68388.html. (Accessed 01/05/2025)
[14] J. Sini, M. et al., “Towards an automatic approach for hardware verification according to ISO 26262 functional safety standard,” 2018 IEEE 24th International Symposium on On-Line Testing And Robust System Design, Platja d’Aro, Spain, 2018, pp. 287-290.
[15] G. Bahig and A. El-Kadi, “Formal Verification of Automotive Design in Compliance With ISO 26262 Design Verification Guidelines,” in IEEE Access, vol. 5, pp. 4505-4516, 2017.
[16] M. I. Hafiz, “Model Based Development Methodology in Compliance with ISO 26262 for Safe Automotive ECU,” 2023 International Conference on Electrical, Computer and Energy Technologies, Cape Town, South Africa, 2023, pp. 1-6.
[17] P. Kilian, O. Koller, P. Van Bergen, C. Gebauer, F. Heidinger and M. Dazer, “Emergency Operation in the Power Supply Domain According to ISO 26262,” in IEEE Access, vol. 10, pp. 47557-47569, 2022.
[18] F. A. da Silva, et al. “An automated formal-based approach for reducing undetected faults in ISO 26262 hardware compliant designs,” 2021 IEEE International Test Conference, Anaheim, USA, 2021, pp. 329-333.
[19] H. Kondo et al., “A 28-nm Automotive Flash Microcontroller With Virtualization-Assisted Processor Supporting ISO26262 ASIL D,” in IEEE Journal of Solid-State Circuits, vol. 55, pp. 133-144, Jan. 2020.